Tailoring the Pore Structure of SBA-16 Silica Molecular Sieve through the Use of Copolymer Blends and Control of Synthesis Temperature and Time

Tae-Wan Kim,[†] Ryong Ryoo,*[,†] Michal Kruk,[‡,§] Kamil P. Gierszal,[‡] Mietek Jaroniec,*[,‡] Satoshi Kamiya,[||] and Osamu Terasaki[||,⊥]

National Creative Research Initiative Center for Functional Nanomaterials, and Department of Chemistry (School of Molecular Science-BK21), Korea Advanced Institute of Science and Technology, Daejeon, 305-701, Korea, Department of Chemistry, Kent State University, Kent, Ohio 44242, Department of Physics, Graduate School of Science and Center for Interdisciplinary Research, Tohoku University, Sendai 980-8578, Japan

Received: March 31, 2004; In Final Form: May 22, 2004

SBA-16 mesoporous silicas with cubic *Im*3*m* structure were synthesized using Pluronic F127 poly(ethylene oxide)−poly(propylene oxide)−poly(ethylene oxide) triblock copolymer ($EO_{106}PO_{70}EO_{106}$) and its blends with Pluronic P123 triblock copolymer ($EO_{20}PO_{70}EO_{20}$) as supramolecular templates. The resulting materials were characterized using X-ray diffraction, transmission electron microscopy, and argon and nitrogen adsorption. Selected samples were also modified with series of organosilanes of gradually increasing sizes and the accessibility of the pore structure after the modification was assessed using argon adsorption, which allowed us to determine the diameter of entrances to the ordered mesopores. It was shown that the pore cage diameter in SBA-16 can be enlarged in a wide range not only by increasing the synthesis temperature and time, as previously known, but also by increasing the content of P123 copolymer in the polymer mixture. These three ways allowed us to synthesize SBA-16 with nominal mesopore diameters from ∼4.5 to 9 nm. Even more importantly, they were also suitable for the tailoring of the pore entrance diameter from ∼1 to at least 6 nm, although in this case, the effect of the copolymer mixture composition on the entrance size was relatively small. In the case of SBA-16 samples synthesized at low temperatures or short hydrothermal treatment times, there was evidence that the pore entrance size was as low as 0.4−0.7 nm, as argon atoms were capable of entering the pore structure, but trimethylchlorosilane appeared to be largely excluded from it. By varying the synthesis temperature, time, and template composition, SBA-16 samples with essentially the same mesopore cage diameter and with largely different pore entrance sizes were synthesized. The present work is a step forward in the synthesis of a mesoporous molecular sieve with independently tailored mesopore diameter and entrance size.

Introduction

Ordered silicas with large (diameter > 5 nm) cage-like mesopores (OSLCMs) have attracted a lot of attention over the last several years.[1−16] These materials have many attractive features, such as (i) the ease of synthesis from commercially available, inexpensive reagents,[10,17] (ii) high specific surface area, (iii) the availability in forms of thin films (with pores accessible from the surface of the film),[18−23] fibers,[24] monoliths,[25] and patterned surfaces,[26] (iv) controlled pore cage[13−15,17,27−29] and entrance[13−15,30,31] dimensions, and (v) high hydrothermal stability.[32] The above features make OSLCMs suitable as catalyst supports,[33,34] templates for nanostructures synthesis,[35] media for immobilization of biomolecules,[36−38] and sensors.[39,40] SBA-16 of cubic *Im*3*m* symmetry (body-centered cubic structure) synthesized using a poly(ethylene oxide)−poly(propylene oxide)−poly(ethylene oxide) triblock copolymer Pluronic F127 ($EO_{106}PO_{70}EO_{106}$) was the first well-documented example of ordered mesoporous silica with cage-like pores of diameter well above 5 nm.[1] The formation of the SBA-16 mesophase was also achieved for somewhat lower EO/PO ratios using mixtures of Pluronic F127 with Pluronic P123 ($EO_{20}PO_{70}EO_{20}$) copolymer.[10] Each mesopore in the body-centered cubic structure has eight nearest neighbor mesopores, and electron crystallography study[5] suggests that each mesopore is actually connected with its eight adjacent pores, thus forming a multidirectional pore network system. Another known cubic structure of OSLCM is a cubic *Pm*3*n* structure of SBA-6 silica templated by a large gemini alkylammonium surfactant.[5] This structure features two kinds of mesopore cages of diameters ∼7.3 and ∼8.5 nm. Interestingly, this is the only currently known example of OSLCM templated by an alkylammonium surfactant. Further work led also to the synthesis of OSLCM with cubic *Fm*3*m* symmetry (face-centered cubic structure). FDU-1 silica[4] with this cubic close-packed structure exhibited irregularities related to the occurrence of hexagonal close-packed stacking sequences,[13] but recently the syntheses of pure cubic *Fm*3*m* structure were claimed.[14,15] The synthesis of hexagonal close-packed structure $P6_3/mmc$ was also reported,[24] but it is yet to be verified whether this is a pure 3-D hexagonal material or it contains a cubic close-packed intergrowth, which was typically

* Corresponding authors. (Ryoo) E-mail: rryoo@kaist.ac.kr. (Jaroniec) Phone: 330-672-3790; Fax: 330-672-3816; E-mail: jaroniec@kent.edu.
† Korea Advanced Institute of Science and Technology.
‡ Kent State University.
§ Current address: Department of Chemistry, Carnegie Mellon University, Pittsburgh, PA 15213.
|| Tohoku University.
⊥ Current address: Arrhenius Laboratory, Stockholm University, 10691 Stockholm, Sweden.

10.1021/jp048582k CCC: $27.50
Published on Web 07/02/2004

observed for silica-based ordered mesoporous materials of hexagonal close-packed structure.[8,41]

The interest in the ordered silicas with cage-like mesopores is fostered to some extent by their fascinating 3-dimensional structures,[5,8] but the major driving force is an expectation that these materials will be useful in many applications, including catalysis, sensing, molecular sieving, templating of nanostructures, immobilization of biomolecules, and so forth. The structures of these silicas feature multidirectional pore systems that are likely to be more resistant to local pore blockage than channel-like pores. Moreover, thin films of ordered silicas with cage-like pores are expected to exhibit pore entrances in the direction perpendicular to the film surface, which is desired in applications as sensors or membrane materials. There are indications that ordered silicas with large cage-like pores can be readily obtained with pore entrance diameters as low as about one nanometer,[30,31] which suggests their suitability as molecular sieves. The actual molecular sieving properties have already been demonstrated for smaller-pore ordered silicas with cage-like mesopores.[42] The tendency to form relatively narrow connections between adjacent mesopores was not helpful in the development of OSLCMs for immobilization of biomolecules, but this problem has recently been overcome by synthesizing materials with large entrances to the mesopores,[38] which can be readily achieved (in the case of the copolymer-templated materials) through the increase in the synthesis temperature or time or addition of micelle expanders.[13,15,38] It is also interesting to note that OSLCMs have recently been extensively studied as model adsorbents,[43−49] providing much insight into gas adsorption behavior in cage-like pores, which is important from the point of view of development of adsorption methods of the structural characterization of porous solids.

The current work shows that OSLCMs with body-centered cubic structures (i.e., SBA-16 silicas) can be synthesized with a wide range of mesopore cage diameters and entrance sizes by using block copolymer mixtures as templates and by controlling synthesis temperature and time. The prospects of independent tailoring of pore cage and entrance size are highlighted. The described strategies for the pore structure design are expected to be generally applicable for other polymer- or oligomer-templated silicas with cage-like mesopores arranged in various structures.

Experimental Section

Materials. SBA-16 silicas were synthesized using poly(ethylene oxide)−poly(propylene oxide)−poly(ethylene oxide) triblock copolymers as supramolecular templates in a way modified with respect to that originally reported by Zhao et al.[1] Pluronic F127 copolymer ($EO_{106}PO_{70}EO_{106}$) and its mixtures with Pluronic P123 copolymer ($EO_{20}PO_{70}EO_{20}$) were used to attain average molar compositions $EO_{106}PO_{70}EO_{106}$, $EO_{90}PO_{70}EO_{90}$, $EO_{80}PO_{70}EO_{80}$, and $EO_{70}PO_{70}EO_{70}$ in a way similar to that reported by Kim et al.[10] Tetraethyl orthosilicate (TEOS, 98%, Acros) was used as the silica source under acidic synthesis conditions. Briefly, an aqueous solution of copolymers was prepared by dissolving in a solution of hydrochloric acid in distilled water. TEOS was then added with magnetic stirring at 308 K. The starting molar composition was 0.0040 F127:1.0 TEOS:4.0 HCl:130 H_2O for $EO_{106}PO_{70}EO_{106}$, 0.00084 P123:0.0038 F127:1 TEOS:4.2 HCl:137 H_2O for $EO_{90}PO_{70}EO_{90}$, 0.0016 P123:0.0037 F127:1.0 TEOS:4.4 HCl:144 H_2O for $EO_{80}PO_{70}EO_{90}$, and 0.0025 P123:0.0034 F127:1.0 TEOS:4.6 HCl:151 H_2O for $EO_{70}PO_{70}EO_{70}$. The mixture was magnetically stirred for about 15 min until TEOS was completely dissolved. The mixture was placed in an oven for 24 h under static condition at 308 K for precipitation of the product. The mixture was further maintained at 333, 353, 373, or 403 K for hydrothermal treatment, whose time was varied from 1 h to 7 days, depending on the particular sample. The white solid precipitate was isolated by filtration without washing and dried at 373 K. Subsequently, the product was calcined under air at 823 K after washing with ethanol in order to remove the copolymer template.

The samples are denoted X*t*-*y*, where X = A, B, C and D for the $EO_mPO_{70}EO_m$ copolymer or copolymer blend with m = 106, 90, 80, and 70, respectively; *t* denotes the temperature of the second step of the synthesis (the hydrothermal treatment) in degrees Kelvin; and *y* denotes the time of the hydrothermal treatment in hours ("h") or days ("d"). For instance, C373-1d denotes a sample synthesized using the $EO_{80}PO_{70}EO_{80}$ template (copolymer mixture) and the hydrothermal treatment time of 1 day at 373 K. The surfaces of selected SBA-16 samples were modified with organosilanes, including trimethylchlorosilane, triethylchlorosilane, tripropylchlorosilane, butyldimethylchlorosilane, hexyldimethylchlorosilane, octyldimethylchlorosilane, decyldimethylchlorosilane, and octadecyldimethylchlorosilane. Typically, 100 mg of the SBA-16 silica was reacted with 1.5 cm^3 of the silane in 10 cm^3 of pyridine under reflux conditions for ∼1 day, which is similar to the method used in our earlier work.[30,31] The product was filtered, washed, and dried in an oven at 353 K for two or more hours. The modified samples are denoted Xt-y−S, where S is TMS, TES, TPS, BDMS, HDMS, ODMS, DDMS, and ODDMS (trimethylsilyl, triethylsilyl, tripropylsilyl, butyldimethylsilyl, hexyldimethylsilyl, octyldimethylsilyl, decyldimethylsilyl, or octadecyldimethylsilyl, respectively). The C373-3d sample was modified first with ODDMS and then with DDMS ligands, and the resulting modified material is denoted C373-3d−ODDMS+DDMS.

Measurements. The X-ray diffraction (XRD) patterns were recorded on a Rigaku Multiplex instrument (operated at 2 kW) using Cu Kα radiation. The transmission electron microscopy (TEM) images were taken from thin edges of particles supported on a porous carbon grid, using a JEOL JEM-3010 equipment operated at 300 kV. The nitrogen and argon adsorption isotherms were measured at 77 K using Micromeritics ASAP 2010 volumetric adsorption analyzers. Before the adsorption measurements, the SBA-16 samples were outgassed under vacuum for 2 h at 473 K, whereas the organosilane-modified SBA-16 samples were outgassed at 413 K. In the case of argon adsorption at 77 K, the saturation vapor pressure for the gas−solid equilibrium (measured periodically during the adsorption measurement) was used to calculate the relative pressure.[48] Weight-change curves were recorded under air on a TA Instruments TGA 2950 high-resolution thermogravimetric analyzer in a high-resolution mode with the maximum heating rate of 5 K min^{-1}.

Calculations. The unit-cell parameter was calculated from the position of the peaks (typically (110) and one or two higher-angle peaks) on the powder XRD patterns. The BET specific surface area[50] was calculated from nitrogen adsorption data in the relative pressure range from 0.04 to 0.2. The total pore volume[50] was estimated from the amount of nitrogen adsorbed at a relative pressure of 0.99. The external surface area and the sum of the micropore volume and primary mesopore volume were calculated using the α_s plot method[51] from the nitrogen adsorption data at pressures following the capillary condensation step.[17] It should be noted that the IUPAC classification of pores on the basis of their width is adopted herein, according to which

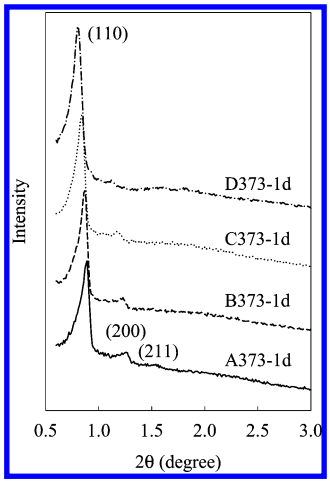

Figure 1. XRD patterns for SBA-16 silicas synthesized using Pluronic F127 block copolymer, and mixtures with different molar ratios of Pluronic F127 and P123 block copolymers, with heating for 1 day at 373 K. A, B, C, and D denote the average polymer compositions of $EO_{106}PO_{70}EO_{106}$, $EO_{90}PO_{70}EO_{90}$, $EO_{80}PO_{70}EO_{80}$, and $EO_{70}PO_{70}EO_{70}$, respectively.

pores of width below 2, between 2 and 50, and above 50 nm are classified as micropores, mesopores, and macropores, respectively.[50] Ordered spherical mesopores of SBA-16 are referred to as primary mesopores. The microporosity in SBA-16 is constituted by (i) the micropores originating from the occlusion of the poly(ethylene oxide) chains in the silica walls[52,53] during the SBA-16 formation, and (ii) the entrances to the cage-like mesopores, if the latter are in the micropore size range. The pore size distributions (PSDs) were calculated from nitrogen and argon adsorption data using a method calibrated for cylindrical mesopores.[54,55] Therefore, the diameter of the spherical mesopores of SBA-16 is likely to be underestimated by about 2 nm, as inferred from earlier studies.[13]

Results and Discussion

X-ray Diffraction. Shown in Figure 1 are XRD patterns for SBA-16 silicas synthesized using F127 block copolymer ($EO_{106}PO_{70}EO_{106}$) and its mixtures with P123 block copolymer ($EO_{20}PO_{70}EO_{20}$), which provided the average length of 90, 80, and 70 units in the poly(ethylene oxide) blocks. It can be seen that the addition of the block copolymer with shorter poly(ethylene oxide) chain caused the shift of the XRD reflections toward lower angles, which provided evidence of an increase in the unit-cell parameter (see Table 1). All the XRD patterns are similar to one another and can be indexed on the cubic *Im*3*m* structure. The increase in the unit-cell parameter with retention of the *Im*3*m* structure was also achieved through the increase of the time or temperature of the hydrothermal treatment (see XRD patterns shown in Supporting Information Figures 1S and 2S and unit-cell parameters listed in Table 1). The latter results are expected on the basis of earlier studies of copolymer-templated OSLCMs.[13−15] The increase in the unit-cell parameter was accompanied by changes in the relative intensity of XRD reflections, and in particular, (200) reflection, which was clearly observed for most of the samples, was not resolved for two samples, one synthesized at the longest time (C373-7d) and the other at the highest hydrothermal treatment temperature (C403-1d). In cases of the latter two samples, the *Im*3*m* structure cannot be ascertained on the basis of these XRD patterns with single peaks, but the sequence of changes in the XRD patterns with time and temperature of the synthesis does not provide any indication that the structure symmetry for the two samples considered may be different from that of the other samples.

TABLE 1: Structural Properties of SBA-16 Silicas[a]

sample	a (nm)	S_{BET} ($m^2\ g^{-1}$)	V_t ($cm^3\ g^{-1}$)	$V_p + V_{mi}$ ($cm^3\ g^{-1}$)	S_{ex} ($m^2\ g^{-1}$)	w_{KJS}[b] (nm)
A373-1d	14.0	790	0.47	0.47	<10	5.6 (5.5)
B373-1d	14.4	800	0.51	0.50	10	6.2 (6.0)
C373-1d	15.0	810	0.53	0.52	<10	6.7 (6.5)
D373-1d	15.6	740	0.56	0.48	40	7.3 (7.0)
C373-1h	13.3	370	0.21	0.20	<10	4.7 (4.7)
C373-3h	14.0	590	0.34	0.33	<10	5.7 (5.5)
C373-12h	15.0	790	0.52	0.50	20	6.7 (6.4)
C373-3d	16.1	780	0.63	0.62	10	7.5 (7.2)
C373-7d	16.5	620	0.67	0.55	70	8.4 (7.9)
C333-1d	14.2	380	0.26	0.23	20	5.5 (5.4)
C353-1d	14.6	540	0.36	0.34	20	6.1 (6.0)
C403-1d	16.8	580	0.72	0.70	10	8.9 (8.2)

[a] Notation: a, unit-cell parameter; S_{BET}, BET specific surface area; V_t, total pore volume; $V_p + V_{mi}$, the sum of primary mesopore volume and micropore volume; S_{ex}, external surface area; w_{KJS}, the pore diameter calculated using the KJS method for cylindrical pores (the values in parentheses were calculated from argon adsorption data; the actual diameter of spherical pores of SBA-16 is likely to be about 2 nm higher than the values provided).

Transmission Electron Microscopy. The structural assignment of samples A373-1d and D373-1d as materials with a body-centered cubic structure was confirmed by TEM. Shown in Figure 2 are TEM images corresponding to [100], [110], and [111] projections of body-centered cubic (*Im*3*m*) structure and the corresponding electron diffraction (ED) patterns (insets in Figure 2a−c) for sample A373-1d. The TEM images, which are similar to those reported earlier for highly ordered SBA-16, whose structure had been solved using the electron crystallography,[5] revealed a high degree of structural perfection in sample A373-1d, which was additionally confirmed by the fact that the ED patterns were very well resolved. The structures of samples A373-1d and D373-1d were determined using the electron crystallography method.[5] The obtained electron potential maps of (110) sections of the samples (plotted for a full range of ratios of the primary pore volume to the unit cell volume) are shown in Figure 3. The comparison of these maps indicates that sample A373-1d has lower mesopore diameter and thicker pore walls (relative to the pore diameter) than sample D373-1d. A more exact interpretation would depend on the choice of the threshold value for the electron potential between the pore and the wall. In principle, it is possible to determine the threshold value on the basis of the ratio of pore volume to the pore wall volume. In the case of materials templated by copolymers with poly(ethylene oxide), there is typically some disordered microporosity in the pore walls.[52] Therefore, the pore wall volume (per gram of material) is not simply a reciprocal of the framework density (which can be determined from helium picnometry), but includes an additional component of the micropore volume. The latter can often be obtained from gas adsorption data using a comparative plot method,[52] but in the case of SBA-16 samples under study, the shape of the comparative plots precluded the elucidation of the micropore volume with a reasonable accuracy, which was probably related to the overlap of micropore filling with adsorption in the entrances to the pores. Therefore, the determination of the threshold value between the pore wall and the void pore space for the electron potential maps presented here was not attempted.

Argon Adsorption. Argon adsorption isotherms for the SBA-16 silicas synthesized using different copolymer template compositions, hydrothermal treatment times, and temperatures are shown in Figures 4−6. All the isotherms featured more or

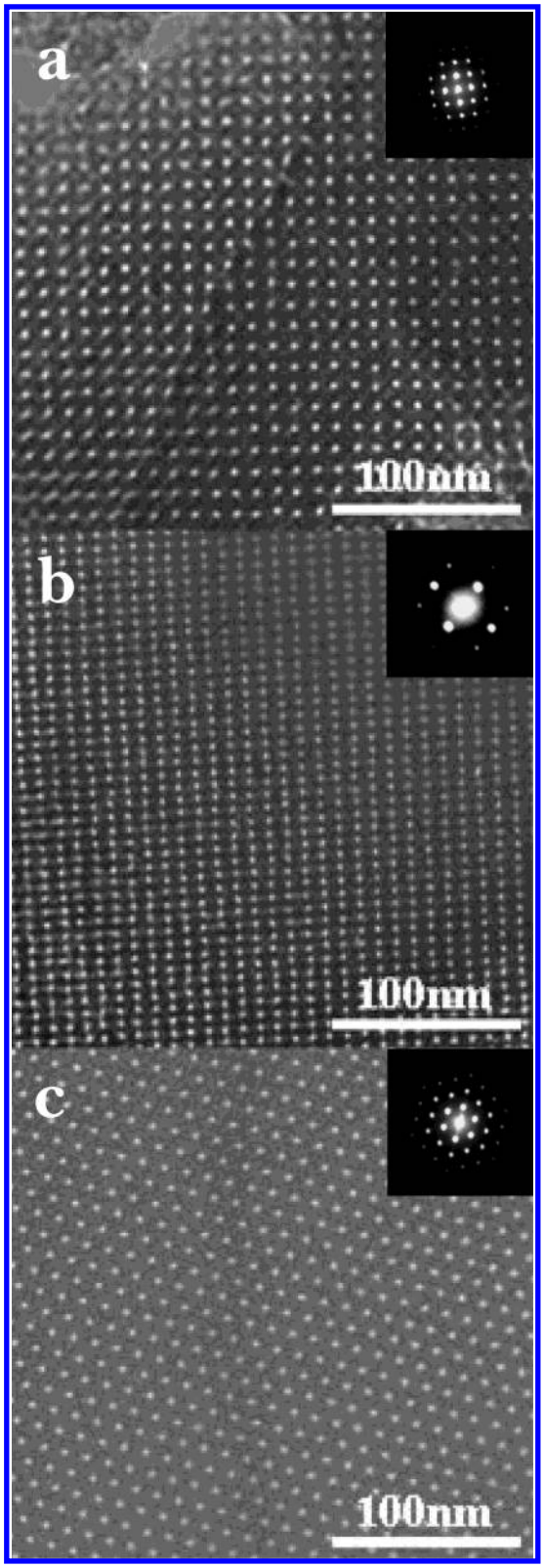

Figure 2. TEM images of the SBA-16 silica A373-1d: (a) [100], (b) [110], and (c) [111] projections.

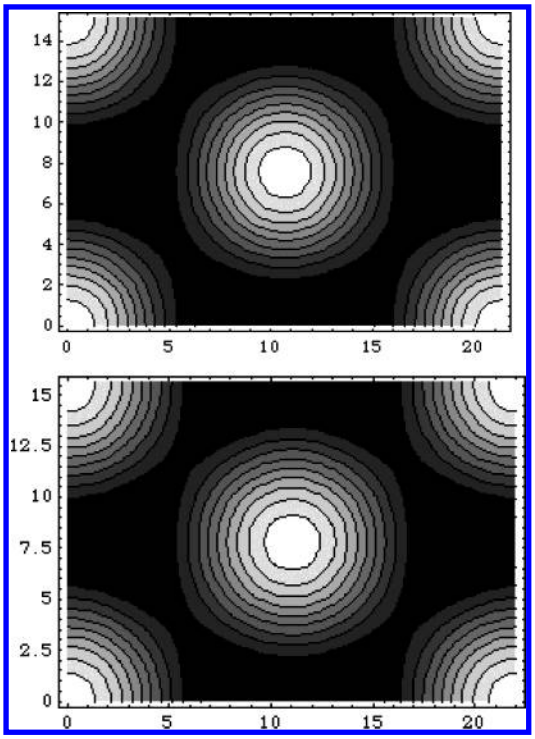

Figure 3. Electron potential maps of (110) sections of samples A373-1d (top) and D373-1d (bottom) plotted for a full range of ratios of the primary pore volume to the unit cell volume.

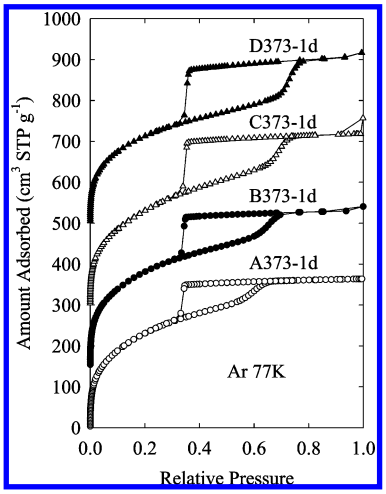

Figure 4. Argon adsorption isotherms for SBA-16 silicas synthesized using Pluronic F127 and mixtures of Pluronic F127 and P123 with different molar ratios. The isotherms for samples B373-1d, C373-1d, and D373-1d were offset vertically by 150, 300, and 500 cm^3 STP g^{-1}, respectively.

less pronounced capillary condensation steps at relative pressures somewhere between 0.45 and 0.85, which indicate the presence of uniform mesopores.[13] The isotherms leveled off at pressures following the capillary condensation. It should be noted that steep increases in the amount adsorbed observed in the proximity of the saturation vapor pressure (relative pressure close to 1) for several of the samples are likely to be related to the formation of bulk solid argon in the sample tube and thus do not provide any structural information about the considered materials (this conjecture is consistent with the nitrogen adsorption data shown in Supporting Information Figures 3S−5S). The fact that the amount adsorbed below the onset of capillary condensation was higher (usually much higher) than the increase in adsorption due to capillary condensation suggests that the lower-pressure adsorption was not only due to multilayer adsorption on the surface of ordered mesopores, but also to the micropore filling. This is consistent with earlier findings that silica frameworks templated by oligomers or block copolymers with EO_n blocks tend to exhibit microporosity, which is constituted by voids originally occupied by EO_n blocks occluded in the silica matrix, as clarified in our earlier studies.[52,53]

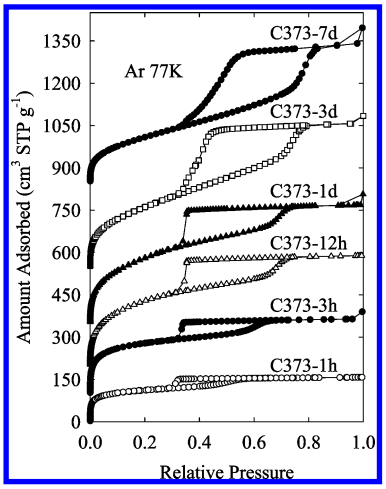

Figure 5. Argon adsorption isotherms for SBA-16 silicas synthesized using a mixture of Pluronic F127 and P123 with average composition of $EO_{80}PO_{70}EO_{80}$ in a two-step synthesis involving the heating at 373 K for different periods of time. The isotherms for samples C373-3h, C373-12h, C373-1d, C373-3d, and C373-7d were offset vertically by 100, 200, 350, 550, and 850 cm^3 STP g^{-1}, respectively.

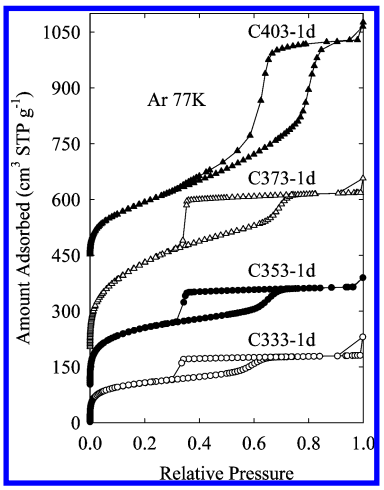

Figure 6. Argon adsorption isotherms for SBA-16 silicas synthesized using a mixture of Pluronic F127 and P123 with average composition of $EO_{80}PO_{70}EO_{80}$ in a two-step synthesis involving the heating at different temperatures. The isotherms for samples C353-1d, C373-1d, and C403-1d were offset vertically by 100, 200, and 450 cm^3 STP g^{-1}, respectively.

For all samples, the desorption branches of the argon isotherms did not follow the adsorption branches, that is, adsorption−desorption hysteresis was observed. In general, in cases where the capillary condensation of argon or nitrogen at 77 K is observed above a certain relative pressure (referred to as the lower limit of adsorption−desorption hysteresis), the hysteresis loops are observed.[44,48−50] In the case of adsorption and desorption in cylindrical mesopores, the hysteresis loop tends to be quite narrow and both capillary condensation pressure and capillary evaporation pressure tend to be increasing functions of the pore diameter, as demonstrated experimentally using ordered materials with approximately cylindrical pores.[54,55] It needs to be noted here that the experimental relation between the pore diameter and the capillary evaporation pressure is less unique, most likely because of the effect of constrictions in the cylindrical mesopores, which would cause the delayed capillary evaporation.[54,55] In the case of cage-like mesopores, the capillary condensation pressure is an increasing function of the pore cage diameter (analogous to the case of cylindrical pores).[43,48] However, the capillary evaporation pressure tends to reflect

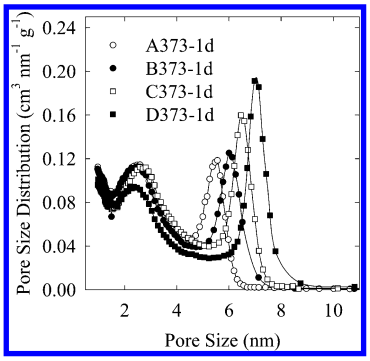

Figure 7. Pore size distributions calculated from argon adsorption data for SBA-16 silicas synthesized using Pluronic F127 and mixtures of Pluronic F127 and P123 with different molar ratios.

either the size of the largest entrance to the given mesopore (if evaporation takes place above the lower limit of hysteresis) or the upper limit of possible entrance sizes (if evaporation takes place at the lower limit of hysteresis).[48] This is because the emptying of interiors of cage-like mesopores cannot take place when these interiors do not have a direct access to the surrounding gas phase through a continuous pathway of gas phase. The exception is the case where the lower limit of hysteresis is reached, at which point the capillary evaporation from the interiors of mesopores takes place even if the connecting pores are still filled with the liquid-like adsorbate phase.

The significant width of the hysteresis loops observed for the SBA-16 samples studied herein suggests a cage-like pore shape,[43,48] which is known to be characteristic of ordered mesopores of SBA-16.[5] In most cases, the hysteresis loops closed sharply at relative pressures corresponding to the lower limit of the adsorption−desorption hysteresis (a relative pressure range 0.26−0.38 for argon at 77 K). As discussed elsewhere, this behavior indicates that that the diameter of entrances to the ordered mesopores is smaller than ∼4 nm.[44,48,49] This is consistent with the pore entrance diameter estimate of 2.3 nm reported earlier on the basis of electron crystallography for an SBA-16 silica sample synthesized under certain conditions.[5] However, in the cases of samples hydrothermally treated for long times (3 and 7 days) or at higher temperature (403 K), the hysteresis loops gradually closed above the lower limit of hysteresis, which indicates the pore entrance diameters above ∼4 nm and thus more open pore structures.[13,48] The fact that the descending parts of the desorption branches of hysteresis loops were quite steep indicates that the size distribution of pore entrances (more specifically, the distribution of the widest entrances to particular mesopores) is quite narrow. The comparison of the position of the desorption branches of hysteresis loops for these SBA-16 samples with the position of desorption branches for materials with cylindrical pores of known diameter[48] leads to a conclusion that samples the C373-3d and C373-7d exhibited pore entrances of diameter in the range ∼4−5 nm, whereas the entrance size in the C403-1d sample is ∼6−7 nm.

The position of the capillary condensation steps on the isotherms shifted to higher relative pressures, and thus the mesopore diameter increased, as (i) the average EO_n block length decreased; (ii) the hydrothermal treatment time increased; or (iii) the hydrothermal treatment temperature increased. The pore size distributions (PSDs) shown in Figures 7−9 reflect these effects. The first of these three ways was suitable for systematically increasing the mesopore diameter by up to ∼1.5 nm (from 5.6 to ∼7 nm; see Table 1). The second one allowed us to tailor the pore size within a ∼3 nm interval from 4.7 to ∼8 nm, and

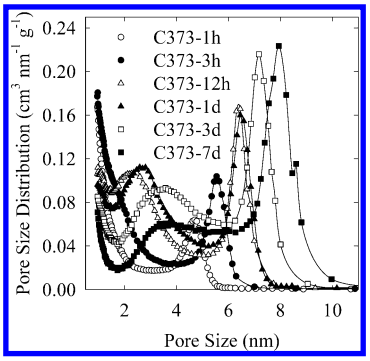

Figure 8. Pore size distributions calculated from argon adsorption data for SBA-16 silicas synthesized using a mixture of Pluronic F127 and P123 with average composition of $EO_{80}PO_{70}EO_{80}$ in a two-step synthesis involving the heating at 373 K for different periods of time.

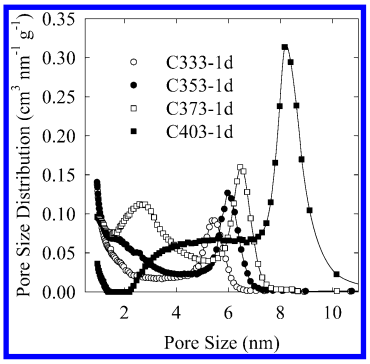

Figure 9. Pore size distributions calculated from argon adsorption data for SBA-16 silicas synthesized using a mixture of Pluronic F127 and P123 with average composition of $EO_{80}PO_{70}EO_{80}$ in a two-step synthesis involving the heating at different temperatures.

the third one within a ~3 nm interval from 5.5 to more than 8 nm. Taking into account that these mesopore diameters are likely to be systematically underestimated by about 2 nm due to the calculation procedure employed,[13] the obtained results demonstrate the opportunity of custom-tailoring of SBA-16 pore diameter from ~6.5 to more than 10 nm. The mesopore diameter enlargement as the hydrothermal treatment temperature increases has been reported first for disordered silicas with uniform mesopores templated by oligomeric surfactants.[56] Later, analogous behavior was reported for copolymer-templated silicas with 2-D hexagonally ordered cylindrical mesopores (which were dubbed SBA-15; they form in the presence of Pluronic P123 or other copolymers).[1] Similar results were also reported for copolymer-templated OSLCMs, including SBA-16[27] as well as structures with cubic close-packed symmetry (*Fm*3*m*).[13] The increase in the diameter of mesopores in copolymer-templated silicas as the hydrothermal treatment time is prolonged was apparent from some early results on SBA-15 synthesis,[1] and later was well documented by us in the case of OSLCMs.[13] The observed increase in the pore diameter as the average length of the EO_m block decreased (which was rather unexpected as the increase of the average size of the copolymer macromolecules resulted in the decrease in the mesopore diameter) has a precedent reported just recently for silicas templated using different copolymers.[29] Although the experimental basis of this recent conclusion is not fully reliable due to the possibility of differences in the pore geometry from one sample to another (which may significantly diminish the accuracy of the pore diameters used for comparison), the suggested explanation is plausible. Namely, it is otherwise known[57] for diblock copolymers with different lengths of EO_m blocks and the same size of poly(butylene oxide) block that the micelle aggregation number is approximately proportional to the reciprocal of the square root of the number of units in the EO_m block. The decrease in the micelle aggregation number leads to the decrease in diameter of the cores of the micelles, which is expected to result in the decrease in the mesopore diameter. A similar effect is likely to be operative in our case, that is, the increase in the average length of the PEO blocks is likely to cause the decrease in the micelle aggregation number and consequently the decrease in the diameter of the cores of the micelles, thereby lowering the mesopore diameter. It should be noted that poly(ethylene oxide) blocks are known to be at least partially occluded in the silica walls[52,53,58] and thus the mesopore diameter is indeed expected to be mostly governed by the diameter of poly(propylene oxide) cores of the micelles. However, it is not clear whether the interface between the silica framework and the micelle template is exactly on the interface between the micelle core and corona. Therefore, one needs to keep in mind that the prediction of the pore diameter on the basis of the micelle core size is approximate in nature. In addition, the silica framework usually shrinks upon the template removal,[53] and consequently the mesopore diameters determined after the template removal are smaller than the diameters of the template-filled mesopores of as-synthesized materials.

Nitrogen adsorption data (shown in Supporting Information Figures 3S−5S) were used to calculate the specific surface areas, total pore volumes, external surface areas and sums of the primary mesopore volume and micropore volume, which are provided in Table 1. The composition of the copolymer template was found to have only a minor effect on the specific surface area and the sum of volumes of primary mesopores and micropores. The increase in time of the hydrothermal treatment afforded larger specific surface areas and pore volumes, but very long treatment times (7 days) resulted in the drop of these structural parameters. The increase in the hydrothermal treatment temperature led to the increase in the pore volume and the specific surface area, although the latter structural parameter decreased at high temperatures (403 K). The external surface areas of the SBA-16 samples were found to be low, which indicates that the particles of SBA-16 formed under synthesis conditions studied herein are significantly larger than the unit-cell sizes.

Pore Entrance Size Assessment through Surface Modification/Pore Accessibility Monitoring. An interesting question is how the mesopore cage diameters are related to the dimensions of entrances to the cages. In the case of samples, whose desorption branches of hysteresis loops on argon isotherms were located above the lower limit of hysteresis, the shift of the relative pressure of capillary evaporation paralleled the shift in the capillary evaporation pressure. This indicates that for these samples, the pore entrance diameter increased as the mesopore cage diameter increased.[48] It would be interesting and potentially useful to uncouple these two structural properties, that is, to independently tailor the mesopore cage diameter and entrance diameter. To achieve this goal, it is helpful to have available a reliable and convenient method to determine the pore entrance size. As discussed above, it was possible to make such estimations for three samples under study on the basis of the position of desorption branches of hysteresis loops. However, in cases of the other samples, the desorption branches were located at the lower limit of adsorption−desorption hysteresis, which merely indicated that the pore entrance diameters were below ~4 nm, as discussed elsewhere.[44,48,49] To overcome this limitation in the pore entrance size assessment, a different and somewhat more involved, but still relatively straightforward pore

entrance size estimation method was used.[30,31] This method, which we recently proposed, consists of (i) the modification of the surface of a given silica with cage-like mesopores with a series of surface modifiers of gradually increasing size, (ii) the identification of the smallest modifier that renders the pores inaccessible to certain gas (nitrogen and argon appear to be the most convenient), and (iii) the evaluation of the pore entrance diameter on the basis of the size of the surface modifier and the size of gas atoms or molecules that cannot access the surface-modified material. From the practical point of view, organomonochlorosilanes are appropriate surface modifiers. This is because they form monolayers (rather than multilayers) on silica surface and their coverage can be made sufficiently high that it is justified to assume that the maximum vertical extension of the ligand, which renders the cage-like pores effectively blocked, reflects the pore entrance radius minus the gas atom (or molecule) radius.[30,31]

Selected SBA-16 samples were modified with series of alkylchlorosilanes of gradually increasing alkyl chain length. In the case of smaller chain lengths (one to three carbon atoms), trialkylchlorosilanes were used to introduce monolayers of trialkylsilyl groups. In the case of sufficiently high coverages of these groups, the degree of coiling of the alkyl chains is expected to be smaller than in the case of alkyldimethylsilanes, as the former ligands are more bulky. For longer chain lengths (from four to eighteen carbon atoms), alkyldimethylchlorosilanes were used, because in most cases the corresponding long-chain trialkylchlorosilanes are not readily available commercially. The changes in the pore entrance size with time of the hydrothermal treatment were explored in detail using the surface-modification/pore-accessibility-assessment (SMPAA) procedure. The C373-1h sample that was hydrothermally treated at 373 K for 1 h exhibited such small sizes of entrances to its mesopores that the pore system was effectively blocked after the modification with the smallest organosilane used, that is, after the introduction of trimethylsilyl (TMS) groups (see Supporting Information Figure 6S). The maximum decrease in the pore diameter related to the introduction of organosilyl ligands can be estimated (on the basis of bond lengths) as $0.75 + 2(k - 1) \times 0.125$ [nm] = $0.75 + 0.25(k - 1)$ [nm], where k is the number of carbon atoms in the longest chain of the ligand. The diameter of an argon atom is ~0.4 nm. Consequently, the pore entrance blockage with TMS ligands implies its diameter below ~1.2 nm. There is evidence that the entrances to the mesopores in the C373-1h sample were even narrower, because the pore blockage was attained at a very low coverage of the TMS ligands, as inferred from thermogravimetry (TGA). It appears that TMS was largely excluded from entering the porous system of this sample, and the blockage is primarily due to the modification of the external surface of the material. The diameter of the trimethylchlorosilane is about 0.7 nm (as inferred from data reported in ref 59), so the pore entrance size in the C373-1h sample appears to be smaller or equal to ~0.7 nm (yet larger than 0.4 nm, as this is the size of Ar atoms that are capable of entering the pores of this sample.

The increase in the hydrothermal treatment time to 3 h resulted in the enlargement of the pore entrance. TGA showed that appreciable loadings of TMS, triethylsilyl (TES) and tripropylsilyl (TPS) ligands were introduced during the surface modification. This is because significant weight losses were recorded under air in temperature ranges where the burn-out of the organic groups in these ligands was expected (see Supporting Information Figure 7S). It was also possible to modify the surface of the C373-3h sample with longer-chain silyl groups,

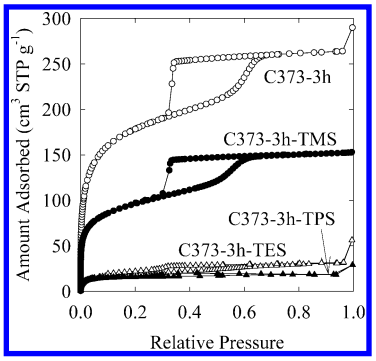

Figure 10. Argon adsorption isotherms for SBA-16 sample C373-3h, unmodified and modified with trimethylsilyl, triethylsilyl, and tripropylsilyl ligands.

such as butyldimethylsilyl (BDMS), hexyldimethylsilyl (HDMS), and octyldimethylsilyl (ODMS). Argon adsorption data showed the porous structure of C373-3h was still accessible after the modification with TMS ligands, and therefore the pore entrance diameters in its structure were at least ~1.2 nm. However, the primary mesopores were essentially completely inaccessible after modifications with TES or larger ligands (see Figure 10 and PSDs in Supporting Information Figure 8S), which indicated that the pore entrance diameters in this sample were below 1.4 nm.

It should be noted here that from its very nature, the pore blocking experiments employed herein provide information about the connectivity of ordered mesopores (or pores in general) with gas phase on the exterior of the material's particles. This connectivity is defined as the existence or absence of percolation pathways, that is, continuous paths, which connect the pores in the particles with the surrounding gas phase. Each of the ordered mesopores in the SBA-16 structure is expected to have eight nearest-neighbor mesopores and to be connected to each of them, and thus multiple percolation pathways from each pore to the surrounding are certainly possible. The inaccessibility of the modified porous structure for a given gas implies that all the percolation pathways from the mesopores to the surrounding were narrowed so much as a result of the modification that they could not be traversed by the gas atoms or molecules used. Therefore, in the case of pore networks with connectivity higher than one (connectivity is the number of entrances to a given pore), the modification experiment provides information about the widest continuous paths of pore entrances, and thus about the widest entrances to particular pores. This implies that the information about the pore entrance size distribution is not obtainable from this experiment. The notion of the pore entrance diameter evaluated using the considered method (as well as on the basis of the analysis of desorption branches of isotherms) should be understood accordingly.

Pore entrances in the SBA-16 structure were further enlarged when the time of the hydrothermal treatment at 373 K was increased to 12 h. In this case, the modification with HDMS ligands did not block the mesopores, and ODMS ligands blocked the mesopores only partially (see Supporting Figure 9S). The application of DDMS ligands was required to completely shut down the access of argon to the pore structure. This suggests that the pore entrance diameters in the C373-12h sample are above 2.4 nm, but below 3.4 nm, with the average values somewhere close to 2.9 nm. In the case of the C373-1d SBA-16 sample hydrothermally treated for 1 day, no evidence of pore blockage was observed after the modification with ODMS ligands, but DDMS ligands made the pores inaccessible (Sup-

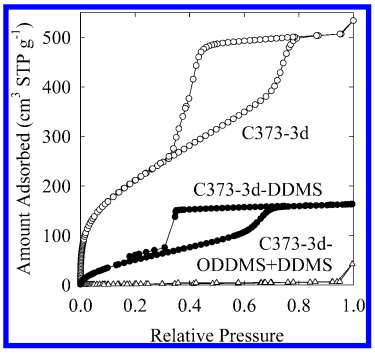

Figure 11. Argon adsorption isotherms for SBA-16 sample C373-3d, unmodified and modified with decyldimethylsilyl, and octadecyldimethylsilyl + decyldimethylsilyl ligands.

porting Figure 10S), and therefore the pore entrance diameters were somewhat larger, approximately between 2.9 and 3.4 nm.

In the case of the SBA-16 sample hydrothermally treated at 373 K for 3 days, it was possible to use desorption branches of hysteresis loops on argon and nitrogen isotherms to estimate that the pore entrance diameter is between 4 and 5 nm. To further verify this contention, the modification of the C373-3d sample with DDMS ligands was carried out. Because of their size, these ligands are not expected to block pores of diameter larger than 3.4 nm, and indeed the ordered mesopores of C373-3d were still accessible after this modification (see Figure 11). In addition, the modification with octadecyldimethylsilyl (ODDMS) ligands was carried out. These ligands have such long chains that they can potentially block pore entrances of diameter up to 5.4 nm. However, in our case, the introduction of the ODDMS ligands was not fully successful, as a low coverage of these groups was attained. No pore blockage was observed, which on the basis of the result discussed hereafter arises from the low surface coverage rather than from the insufficient chain length of the ligands. In the attempt to force the ODDMS groups to assume more extended conformations, the ODDMS-modified SBA-16 was additionally modified with DDMS ligands. This mixed ligand layer effectively shut down the access to the ordered mesopores of the C373-3d material, thus showing that the analysis of desorption branches of hysteresis loops, which led to the estimate of 4−5 nm, provides results consistent with those from the SMPAA procedure (below ∼5.4 nm) for pore entrance diameters for which both of these methods are applicable.

The sequence of the mesopore cage diameter and entrance size changes is illustrated in Scheme 1. The figures show one unit cell in the body-centered structure. The space enclosed by the surface in the unit cell constitutes ordered, approximately cylindrical mesopores of SBA-16 and the connections between these mesopores, whereas the remaining space constitutes the silica walls (which contain additional disordered microporosity). The surfaces shown were generated using the equation $\cos(x) \times \cos(y) + \cos(x) \times \cos(z) + \cos(y) \times \cos(z) = a$ for different values of a ($a < 0$). It was already reported that a similar equation (for $a = 0$) provides a good description of the structure of SBA-16, as determined from electron crystallography.[5]

Earlier study of copolymer-templated ordered silicas with cage-like mesopores showed that the effect of the increase in the hydrothermal treatment temperature tends to be similar to the effect of the increase in the hydrothermal treatment time.[13] The current work is consistent with this observation. The pores of SBA-16 silica hydrothermally treated for 1 day at 333 K became inaccessible to argon after the modification with TMS ligands (see Supporting Figure 11S). TGA data for the obtained

SCHEME 1: Illustration of Changes in SBA-16 Structure Brought About by Increasing the Hydrothermal Treatment Time or Temperature, and by Changing the Relative Proportions of Different Copolymers in the Copolymer Mixture Used as a Template.

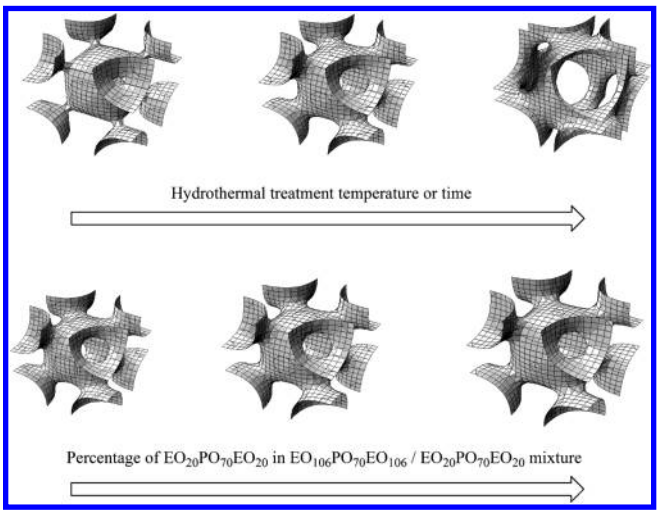

TMS-modified sample indicate a very low loading of TMS ligands, and thus the pore blockage is likely to be a result of the introduction of the ligands primarily on the external surface of the material's particles. This behavior was similar to that described above for the SBA-16 sample hydrothermally treated for 1 h at 373 K and interpreted as evidence of the pore entrance size between 0.4 and 0.7 nm. An SBA-16 sample hydrothermally treated for 1 day at 353 K exhibited a pore blocking behavior quite similar to that of the sample hydrothermally treated for 3 h at 373 K. In particular, the ordered mesopores of both of these materials were accessible after the introduction of TMS ligands, but were largely inaccessible after the modification with TES and TPS ligands. However, in the case of the SBA-16 sample treated at 353 K, small fractions of pores were still accessible after both of these modifications (see Supporting Figures 12S and 13S). Finally, the sample hydrothermally treated for 1 day at 403 K exhibited a quite open pore structure with pore entrances wider than those for the sample hydrothermally treated for 7 days at 373 K, as inferred from the analysis of the desorption branches of gas adsorption isotherms.

The effect of the change in the composition of the copolymer template on the pore entrance size appeared to be quite small. In particular, the pores of the A373-1d sample synthesized using pure F127 copolymer ($EO_{106}PO_{70}EO_{106}$) were accessible after the modification with HDMS ligands, but blocked by somewhat longer ODMS ligands (see adsorption isotherms in Supporting Information Figure 14S and PSD in Supporting Figure 15S; the TGA data shown in Supporting Figure 16S show that the modifications successfully introduced large coverages of ligands). These results suggest that the pore entrance diameters in the A373-1d sample are approximately in the range from 2.4 to 2.9 nm. Essentially the same behavior was also observed for sample D373-1d, although a small fraction of pores was still accessible after the modification with ODMS ligands (see adsorption isotherms in Supporting Figure 17S and PSD in Supporting Figure 18S). The behavior of these two samples was quite similar to the behavior of the C373-1d sample synthesized using a mixture of F127 and P123 copolymers with average formula $EO_{80}PO_{70}EO_{80}$, whose pore structure was accessible after the modification with ODMS ligands, but blocked by slightly longer DDMS groups, which indicates the pore entrance

size of about 2.9−3.4 nm. Interestingly, PSD calculations from argon adsorption data for the samples synthesized using different copolymer mixtures (Figure 7) feature peaks at around 2.5 nm, which is fairly consistent with the above pore entrance size estimates. The peak for the C373-1d sample had a maximum at somewhat larger pore sizes in comparison to those for A373-1d and D373-1d, additionally suggesting that these peaks may be related to the pore entrance size. This is despite the fact that the model used for the PSD calculations is not fully reliable for the considered pore geometry and, in general, it may be difficult to develop a model for accurate PSD calculations for pore geometries illustrated in Scheme 1.[13] Anyway, it is clear that the change of the copolymer composition in the range studied here did not result in any appreciable pore entrance size change, whereas it had a significant impact on the pore cage diameter.

It is important to note that the different ways of structural tailoring depicted in Scheme 1 allow one to obtain samples with a similar mesopore cage diameter, but significantly different pore entrance size. In particular, C373-3h, C333-1d, and A373-1d exhibit very similar nominal pore diameters (about 5.5 nm), but differ significantly in their pore entrance diameters (1.2−1.4 nm, <0.7 nm and 2.4−2.9 nm, respectively, as inferred from SMPAA). This result suggests that the tuning of the synthesis conditions and the template composition should allow one to obtain a range of true mesoporous molecular sieves with independently tailored mesopore cage diameter and entrance size.

Reason for Pore Entrance Enlargement with Temperature/Time. The pore entrance diameter increase as a function of hydrothermal treatment temperature is likely to be related to the known phenomenon of the decrease in hydrophilicity of EO_m blocks as the temperature increases.[1] In the structure of the block copolymer/silica composite (as-synthesized SBA-16), the cores of the (spherical) micelles are constituted by PO_n blocks, whereas the micelle corona, which consists of EO_m blocks, interacts with the silica framework.[52,53,58] At lower temperature, EO_m blocks are expected to favorably interact with hydrophilic silica species and thus to have a tendency to be intimately mixed with the silica framework. When the copolymer/silica composite is subjected to the treatment at higher temperatures, these interactions become less favorable, which is expected to lead to a higher degree of aggregation of EO_m blocks in the silica wall. This aggregation, that is the formation of bundles of EO_m chains and/or the increase in the number of chains in particular bundles, is likely to lead to the increase in the diameter of bridges of EO_m chains between the adjacent micelles in the ordered silica framework. This may lead to the increase in the pore entrance size with time, because the space occupied by these bridges becomes the pore space that connects the adjacent ordered mesopore cages after the removal of the copolymer (because of the fact that the polymer removal leads to shrinkage of the silica framework, the sizes of the connecting pores are likely to be smaller than the sizes of polymer-filled voids). As the hydrothermal treatment is prolonged, the extent of aggregation of EO_m blocks may also increase, leading to the pore entrance size enlargement.

Relation between Capillary Condensation Pressure and Lower Limit of Hysteresis. The adsorption data presented herein are suitable for examining the relation between the lower limit of adsorption−desorption hysteresis and the pore diameter, the latter being reflected by the capillary condensation pressure. It is often assumed that the lower limit of hysteresis, that is the lower closure point of the hysteresis loop, is a function of the adsorbate and temperature.[44] It was also recently suggested that the lower limit of hysteresis depends on the pore shape.[44] Our earlier work indicated the dependence of the lower pressure limit of hysteresis on the pore diameter.[48,55,60] The results for SBA-16 silicas strongly suggest that this is actually the case. Shown in Supporting Information Figure 19S are pressures of capillary evaporation at the lower limit of hysteresis (vertical drops on the isotherms) as a function of the capillary condensation pressure (which is related to the pore diameter) for argon and nitrogen at 77 K. It is clear that the mesopores that exhibit capillary condensation at lower pressures also have a lower limit of hysteresis at somewhat lower pressures. So, the lower limit of adsorption−desorption hysteresis should not be regarded as a single pressure value for a particular gas at particular temperature for a particular pore shape, but as a pressure interval, whose lower boundary corresponds to the smallest mesopores that still exhibit adsorption−desorption hysteresis.

The data shown in Supporting Figure 19S appear to exhibit some scatter, but these apparent irregularities may actually be related to the fact that cage-like pores are not just spheres, but have entrances (see Scheme 1) that may also affect the adsorption behavior. Thus the adsorption behavior of cage-like pores is likely to be a function not only of pore diameter, but also entrance size (and number of entrances), especially when the latter size is relatively large. To this end, the variation in capillary evaporation pressures corresponding to the capillary condensation relative pressures of ∼0.60 (Ar) and ∼0.56 (N_2) can be traced back to largely different pore entrance diameters for the considered samples (C333-1d, C373-3h, and A373-1d). It seems that the more open pore structure (that is, larger pore entrance size) shifts the pressure of capillary evaporation at the lower limit of hysteresis to higher relative pressures. This is consistent with an observation (based on the data presented here and our earlier results) that the lower limit of hysteresis in cage-like mesopores appears to be shifted to somewhat lower pressures in comparison to the limit for cylindrical mesopores.

Conclusions

SBA-16 silica of *Im*3*m* structure is a robust copolymer-templated ordered mesoporous material, whose mesopore cage diameter and pore entrance size can be tailored using several synthesis strategies. The use of mixed copolymer supramolecular templates adds another dimension of the structural design, which in combination with the known approaches based on the control of the synthesis time and temperature provides an opportunity for independent adjustment of the mesopore cage diameter and entrance size. The pore entrance size in SBA-16 can be tailored from subnanometer range to at least 6 nm, making this silica a true mesoporous molecular sieve. The structural changes that SBA-16 undergoes during the hydrothermal treatment are very similar to those reported earlier for other copolymer-templated silicas with cage-like mesopores, which provides evidence of a common behavior of silicas templated by copolymers with poly(ethylene oxide) blocks. Therefore, we suggest that the present synthesis strategy using copolymer mixtures and hydrothermal treatments is suitable for the design of other OSLCMs with controlled pore apertures and inner diameters.

Acknowledgment. R.R. acknowledges support from Creative Research Initiative Program of the Korean Ministry of Science and Technology, and School of Molecular Science through the Brain Korea 21 project. M.J. acknowledges support by NSF Grant CHE-0093707.

Supporting Information Available: Figures (19): figures (2) with experimental XRD data; figures (10) with experimental

gas adsorption data; figures (2) with PSDs derived from adsorption data; figures (4) with experimental TGA data; and figure (1) with the experimental relation between the capillary condensation pressure and the pressure of capillary evaporation at a lower limit of adsorption−desorption hysteresis. This material is available free of charge via the Internet at http://pubs.acs.org.

References and Notes

(1) Zhao, D.; Huo, Q.; Feng, J.; Chmelka, B. F.; Stucky, G. D. *J. Am. Chem. Soc.* **1998**, *120*, 6024.

(2) Kramer, E.; Forster, S.; Goltner, C.; Antonietti, M. *Langmuir* **1998**, *14*, 2027.

(3) Zhang, W.; Glomski, B.; Pauly, T. R.; Pinnavaia, T. J. *Chem. Commun.* **1999**, 1803.

(4) Yu, C.; Yu, Y.; Zhao, D. *Chem. Commun.* **2000**, 575.

(5) Sakamoto, Y.; Kaneda, M.; Terasaki, O.; Zhao, D. Y.; Kim, J. M.; Stucky, G. D.; Shin, H. J.; Ryoo, R. *Nature* **2000**, *408*, 449.

(6) Kipkemboi, P.; Fogden, A.; Alfredsson, V.; Flodstrom, K. *Langmuir* **2001**, *17*, 5398.

(7) Tattershall, C. E.; Jerome, N. P.; Budd, P. M. *J. Mater. Chem.* **2001**, *11*, 2979.

(8) Sakamoto, Y.; Diaz, I.; Terasaki, O.; Zhao, D.; Perez-Pariente, J.; Kim, J. M.; Stucky, G. D. *J. Phys. Chem. B* **2002**, *106*, 3118.

(9) Tattershall, C. E.; Aslam, S. J.; Budd, P. M. *J. Mater. Chem.* **2002**, *12*, 2286.

(10) Kim, J. M.; Sakamoto, Y.; Hwang, Y. K.; Kwon, Y.-U.; Terasaki, O.; Park, S.-E.; Stucky, G. D. *J. Phys. Chem. B* **2002**, *106*, 2552.

(11) Yu, C.; Tian, B.; Fan, J.; Stucky, G. D.; Zhao, D. *J. Am. Chem. Soc.* **2002**, *124*, 4556.

(12) Tian, B.; Liu, X.; Zhang, Z.; Tu, B.; Zhao, D. *J. Solid State Chem.* **2002**, *167*, 324.

(13) Matos, J. R.; Kruk, M.; Mercuri, L. P.; Jaroniec, M.; Zhao, L.; Kamiyama, T.; Terasaki, O.; Pinnavaia, T. J.; Liu, Y. *J. Am. Chem. Soc.* **2003**, *125*, 821.

(14) Fan, J.; Yu, C.; Gao, F.; Lei, J.; Tian, B.; Wang, L.; Luo, Q.; Tu, B.; Zhou, W.; Zhao, D. *Angew. Chem., Int. Ed.* **2003**, *42*, 3146.

(15) Kleitz, F.; Liu, D.; Anilkumar, G. M.; Park, I.-S.; Soloviov, L. A.; Shmakov, A. N.; Ryoo, R. *J. Phys. Chem. B* **2003**, *107*, 14296.

(16) Newalkar, B. L.; Komarneni, S.; Turaga, U. T.; Katsuki, H. *J. Mater. Chem.* **2003**, *13*, 1710.

(17) Matos, J. R.; Mercuri, L. P.; Kruk, M.; Jaroniec, M. *Langmuir* **2002**, *18*, 884.

(18) Zhao, D.; Yang, P.; Melosh, N.; Feng, J.; Chmelka, B. F.; Stucky, G. D. *Adv. Mater.* **1998**, *10*, 1380.

(19) Yu, K.; Hurd, A. J.; Eisenberg, A.; Brinker, C. J. *Langmuir* **2001**, *17*, 7961.

(20) Alberius, P. C. A.; Frindell, K. L.; Hayward, R. C.; Kramer, E. J.; Stucky, G. D.; Chmelka, B. F. *Chem. Mater.* **2002**, *14*, 3284.

(21) Soler-Illia, G. J. A. A.; Crepaldi, E. L.; Grosso, D.; Durand, D.; Sanchez, C. *Chem. Commun.* **2002**, 2298.

(22) Besson, S.; Ricolleau, C.; Gacoin, T.; Jacquiod, C.; Boilot, J.-P. *Microporous Mesoporous Mater.* **2003**, *60*, 43.

(23) Kim, Y.-S.; Kusakabe, K.; Yang, S.-M. *Chem. Mater.* **2003**, *15*, 612.

(24) Yang, P.; Zhao, D.; Chmelka, B. F.; Stucky, G. D. *Chem. Mater.* **1998**, *10*, 2033.

(25) Melosh, N. A.; Davidson, P.; Chmelka, B. F. *J. Am. Chem. Soc.* **2000**, *122*, 823.

(26) Yang, P.; Deng, T.; Zhao, D.; Feng, P.; Pine, D.; Chmelka, B. F.; Whitesides, G. M.; Stucky, G. D. *Science* **1998**, *282*, 2244.

(27) Kao, C.-P.; Lin, H.-P.; Chao, M.-C.; Sheu, H.-S.; Mou, C.-Y. *Stud. Surf. Sci. Catal.* **2001**, *135* (on CD-ROM).

(28) Van Der Voort, P.; Benjelloun, M.; Vansant, E. F. *J. Phys. Chem. B* **2002**, *106*, 9027.

(29) Yu, C.; Fan, J.; Tian, B.; Stucky, G. D.; Zhao, D. *J. Phys. Chem. B* **2003**, *107*, 13368.

(30) Kruk, M.; Antochshuk, V.; Matos, J. R.; Mercuri, L. P.; Jaroniec, M. *J. Am. Chem. Soc.* **2002**, *124*, 768.

(31) Antochshuk, V.; Kruk, M.; Jaroniec, M. *J. Phys. Chem. B* **2003**, *107*, 11900.

(32) Kruk, M.; Celer, E. B.; Jaroniec, M. *Chem. Mater.* **2004**, *16*, 698.

(33) Zheng, G.; Zhu, H.; Luo, Q.; Zhou, Y.; Zhao, D. *Chem. Mater.* **2001**, *13*, 2240.

(34) Huang, L.; Wind, S. J.; O'Brien, S. P. *Nano Lett.* **2003**, *3*, 299.

(35) Tian, B.; Liu, X.; Yang, H.; Xie, S.; Yu, C.; Tu, B.; Zhao, D. *Adv. Mater.* **2003**, *15*, 1370.

(36) Deere, J.; Magner, E.; Wall, J. G.; Hodnett, B. K. *Chem. Commun.* **2001**, 465.

(37) Han, Y.-J.; Watson, J. T.; Stucky, G. D.; Butler, A. *J. Mol. Catal. B: Enzymatic* **2002**, *17*, 1.

(38) Fan, J.; Lei, J.; Wang, L.; Yu, C.; Tu, B.; Zhao, D. *Chem. Commun.* **2003**, 2140.

(39) Wirnsberger, G.; Scott, B. J.; Stucky, G. D. *Chem. Commun.* **2001**, 119.

(40) Yamada, T.; Zhou, H. S.; Uchida, H.; Tomita, M.; Ueno, Y.; Honma, I.; Asai, K.; Katsube, T. *Microporous Mesoporous Mater.* **2002**, *54*, 269.

(41) Hunter, H. M. A.; Garcia-Bennett, A. E.; Shannon, I. J.; Zhou, W.; Wright, P. A. *J. Mater. Chem.* **2002**, *12*, 20.

(42) Garcia-Bennett, A. E.; Williamson, S.; Wright, P. A.; Shannon, I. J. *J. Mater. Chem.* **2002**, *12*, 3533.

(43) Ravikovitch, P. I.; Neimark, A. V. *Langmuir* **2002**, *18*, 1550.

(44) Ravikovitch, P. I.; Neimark, A. V. *Langmuir* **2002**, *18*, 9830.

(45) Vishnyakov, A.; Neimark, A. V. *Langmuir* **2003**, *19*, 3240.

(46) Morishige, K.; Tateishi, N.; Fukuma, S. *J. Phys. Chem. B* **2003**, *107*, 5177.

(47) Morishige, K.; Tateishi, N. *J. Chem. Phys.* **2003**, *119*, 2301.

(48) Kruk, M.; Jaroniec, M. *Chem. Mater.* **2003**, *15*, 2942.

(49) Kruk, M.; Matos, J. R.; Jaroniec, M. *Colloids Surf. A: Physicochem. Aspects*, in press.

(50) Sing, K. S. W.; Everett, D. H.; Haul, R. A. W.; Moscou, L.; Pierotti, R. A.; Rouquerol, J.; Siemieniewska, T. *Pure Appl. Chem.* **1985**, *57*, 603.

(51) Jaroniec, M.; Kruk, M.; Olivier, J. P. *Langmuir* **1999**, *15*, 5410.

(52) Ryoo, R.; Ko, C. H.; Kruk, M.; Antochshuk, V.; Jaroniec, M. *J. Phys. Chem. B* **2000**, *104*, 11465.

(53) Kruk, M.; Jaroniec, M.; Ko, C. H.; Ryoo, R. *Chem. Mater.* **2000**, *12*, 1961.

(54) Kruk, M.; Jaroniec, M.; Sayari, A. *Langmuir* **1997**, *13*, 6267.

(55) Kruk, M.; Jaroniec, M. *J. Phys. Chem. B* **2002**, *106*, 4732.

(56) Prouzet, E.; Pinnavaia, T. J. *Angew. Chem., Int. Ed. Engl.* **1997**, *36*, 516.

(57) Booth, C.; Attwood, D. *Macromol. Rapid Commun.* **2000**, *21*, 501.

(58) Melosh, N. A.; Lipic, P.; Bates, F. S.; Wudl, F.; Stucky, G. D.; Fredrickson, G. H.; Chmelka, B. F. *Macromolecules* **1999**, *32*, 4332.

(59) Zhao, X. S.; Lu, G. Q.; Whittaker, A. K.; Millar, G. J.; Zhu, H. Y. *J. Phys. Chem. B* **1997**, *101*, 6525.

(60) Kruk, M.; Jaroniec, M.; Kim, T.-W.; Ryoo, R. *Chem. Mater.* **2003**, *15*, 2815.